ISSN 0915-633X

NATIONAL INSTITUTE FOR FUSION SCIENCE

Pair Creation of Negative and Positive Pionlike (Muonlike) Particle by Interaction between an Electron Bunch and a Positive Ion Bunch

J. Uramoto

(Received - Oct. 7, 1997)

NIFS-529 Dec. 1997

RESEARCH REPORT
NIFS Series

NAGOYA, JAPAN

Pair Creation of Negative and Positive Pionlike (Muonlike) Particle by interaction between an Electron Bunch and a Positive Ion Bunch

Jōshin URAMOTO

National Institute for Fusion Science
332-6 Orosh-cho, Toki-shi, Gifu, 509-52, Japan

Abstract

Both negative pionlike (π^-) or muonlike (μ^-) particles and positive pionlike (π^+) or muonlike (μ^+) particles are created by an electron bunch and a positive ion bunch which are generated from a low energy (~1 keV) electron beam and a neutral gas, which are detected by a magnetic mass analyzer (MA). Then, the π^- and μ^- particles are detected easily as the apparent current to the beam collector (BC) of MA increases extremely when a positive bias voltage is applied to BC and positive ions are supplied in front of BC. On the other hand, it is difficult to detect the π^+ and μ^+ particles as the apparent current increment on BC and the space charge neutralization inside MA do not occur. It should be noted that the π^+ or μ^+ particles do not penetrate a metal plate while the π^- or μ^- particles penetrate the metal plate easily.

Keywords: negative pionlike particle π^-, positive pionlike particle π^+, apparent current increment.

1. Introduction

It has been reported already[1] that negative pionlike (π^-) particles are extracted from the outside region of the H_2 gas discharge plasma in magnetic fields, and that a special detection method[2),3)] for the π^- particles is necessary. Recently, it is found out[4)] that the apparent current of the π^- particles or the negative muonlike (μ^-) particles to the beam collector BC of the magnetic mass analyzer MA abruptly increases, if positive ions exist around BC and the beam collector bias voltage V_S is positive ($V_S > 0$) with respect to the mass analyzer MA itself. The positive ions are supplied secondarily from reflection of the H^- ions.

On the other hand, the π^- or μ^- particles have produced under a different production method[5)] using an electron beam and a positive ion beam. There, the electron beam is bunched magnetically and the positive ion beam is bunched electrically. In this method, positive ions are supplied also from a secondary plasma (S.P.) around the beam collector BC as shown in Fig. 1 and Fig. 2. In this paper, we will investigate a similar effect for an apparent current of the π^- or μ^- particles to BC when the bias voltage V_S of BC is positive ($V_S > 0$). Moreover, in relation with the apparent current increment of π^- or μ^- and the space charge compensation due to the positive ions from the S.P., a positive pionlike (π^+) or muonlike (μ^+) particle will be researched by reversing the analyzing magnetic field of mass analyzer MA as a pair creation of pionlike or muonlike particle is expected to be produced by interaction between an electron bunch and a positive ion bunch.

2. Ordinary experiment

Schematic diagrams of the experimental apparatus[5)] are shown in Fig. 1 and Fig. 2. The first electron beam (F.E.B.) is stopped critically in front of the entrance slit S by an electrical potential of the decelerator D connected to the cathode of the electron gun. Next, a neutral gas is introduced into the first electron beam region and a plasma is produced through ionization of the gas. Then, positive ions of the plasma are accelerated in front of S, while a positive ion beam with an energy corresponding to the first electron beam acceleration voltage V_A is injected into the magnetic field region through S. Moreover, the stopped beam electrons are reaccelerated electrically toward the gap between two magnetic poles (N) and (S) through S, while the injected ion beam is decelerated electrically and stopped in the gap. The electrically reaccelerated electrons are injected perpendicularly to the magnetic field (B_M) and bunched in cyclotron motions of small radius.

As shown in Fig. 2, the above magnetic system is used as a mass analyzer (MA) of 90° type when the beam collector BC is arranged. The analyzing curvature radius r is 4.3 cm. It should be noted that the back space of the beam collector BC is surrounded by an insulator Ins. to interrupt the diffusion of positive ions from the secondary plasma S.P.[3]. This detection method of pionlike particles has reported already for the H_2 gas discharge plasma[2].

A fringe magnetic field distribution of the analyzing magnetic field B_M under a magnetic coil current of 1A, is shown in Fig. 3 for two different metal plates as the entrance plate (decelerator D) of Fig. 1 and Fig. 2. In this experiment, the iron (Fe) plate is used and the fringe magnetic field is much reduced.

The distribution of electrically applied potential are shown in Fig. 4. The first electron beam from the electron gun is perfectly reflected in front of the entrance slit S of the magnetic mass analyzer MA while a plasma is produced by a gas (air) ionization. Then, a positive ion beam is injected into MA through the slit S and the second electron beam is produced by reacceleration of the plasma electrons. It should be noted that the injected positive ion beam (i_2) is decelerated and stopped electrically, and that the second electron beam (e_2) suffers a magnetron (cyclotron) motion in the uniform magnetic field (which is used as the analyzing magnetic field of MA). As a result, both the electron beam and positive ion beam will be bunched within the small space at the entrance X of the uniform magnetic field.

Thus, we can expect a coherent interaction between the bunched electrons and positive ions.

For the first experiment of Fig. 2, dependences of a negative current I^- to the beam collector BC on the analyzing magnetic field B_M are shown in Fig. 5 for a first electron beam acceleration voltage V_A of 1 kV under a positive bias voltage V_S of the beam collector V_S = 100V. Here, we find that an analyzing relation of the negative muon μ^- is satisfied for the first peak of negative current I^-, if we assume that the effective acceleration voltage V_E is twice of the first electron beam acceleration voltage V_A. That is, the following relation is found: From the analyzing magnetic field B_M where the negative current shows a peak, the curvature radius r of the mass analyzer and the effective acceleration voltage V_E, we can estimate the mass m of the negatively charge particle by,

$$m = \frac{Ze\,(B_M r)^2}{2V_E}$$

$$= \frac{8.8 \times 10^{-2}\, Z\,(B_M r)^2\, m_e}{V_E}, \quad \cdots\cdots (1)$$

where e is the electron charge, B_M is in gauss unit, r is in cm unit, V_E is in volt unit and m_e is the electron mass and Z is the charge number. For the curvature radius $r = 4.3$ cm of this mass analyzer, the Eq. (1) is rewritten by

$$m = \frac{1.63\, Z\, B_M{}^2}{V_E} m_e. \quad \cdots\cdots (2)$$

From Eq. (2) and the experimental conditions for the first peak of I^- of Fig. 5, we obtain $m = m_1 \approx 200\, m_e$ under $V_E = 2V_A = 2$ kV and $B_M \approx 510$ gauss, assuming that $Z = 1$. This experimental result means that negative muonlike particles μ^- are produced (because the typical muon mass is near 207 m_e).

Moreover, we find the second peak of I^- in Fig. 5. From Eq. (2) and the experimental conditions, we obtain $m = m_2 \approx 285\, m_e$ under $V_E = 2$ kV and $B_M \approx 595$ gauss. This mass m_2 is near the typical pion mass (273 m_e). That is, negative pionlike particles π^- are produced also.

3. Net current and Apparent current

To investigate a relation between a net current and an apparent current of the π^- or μ^- particles to the beam collector BC, dependences of a negative current I^- to BC on the analyzing magnetic field B_M are determined in Fig. 6 under two bias voltages of $V_S = 0$V and $V_S = 100$V (at the first electron beam acceleration voltage $V_A = 1$ kV). In Fig. 6, we find that the peaks (corresponding to π^- or μ^-) of the negative current I^- increase about 60 times under the positive bias voltage $V_S = 100$V in comparison with that under $V_S = 0$V. These large apparent increments of negative current peaks under the positive potential $V_S > 0$ of the beam collector BC, may be explained by the following mechanism due to positive ions within the mass analyzer MA and secondary electrons inside BC: The mechanism is shown in Figs. 7 (A) and (B). For $V_S = 0$ of Fig. 7 (A), the negative current I_1^- appears through a closed circuit (π^-, μ^-) — BC — MA. Thus, the I_1^- shows a net current of (π^-, μ^-). Here, we observe a positive ion current to BC when a deep negative bias

voltage ($V_S < -300V$) is given to BC. The positive ions come from the secondary plasma S.P. due to the injected ion beam I.B. and secondary electron beam S.E.B. as shown in Fig. 2. On the other hand, the negative muonlike particle μ^- (decay product of π^- or direct μ^-) inside BC may generate secondary low energy electrons through high energy electrons of the decay process from μ^-. The (back ground) positive ions within MA and the secondary electrons inside BC are shown by +Ion and e_S in Fig. 7 (B). Thus, for $V_S > 0$ of Fig. 7 (B), another closed circuit of negative current I_2^- appears through BC (e_S) — V_S — MA — (+Ion). A total charge of secondary electrons (e_S) due to μ^- may be extremely larger than that of π^- or μ^-. By the above mechanism, the apparent negative current I_2^- for π^- or μ^- increases abruptly in comparison with the net negative current I_1^-.

Thus, we can conclude that the increment mechanism of the apparent negative current is the same with that in the case of H_2 discharge plasma[4].

4. Negative current without positive ion supply

The secondary plasma S.P. as shown in Fig. 2 is produced by the injected positive ion beam I.B. and secondary electron beam S.E.B. while the S.P. diffuses along the weak magnetic field ($B_M \approx 0$) outside the analyzing magnetic field B_M of MA. If a cut plate CP for the secondary plasma S.P. is arranged as shown in Fig. 8 (A), the S.P. can not diffuse near the beam collector BC. Obviously, under this condition, the positive ion current to BC is not observed even if a deep negative bias voltage ($V_S < -300V$) is given to BC. Then, dependences of the negative current I^- to BC on B_M are determined in Fig. 8 (B) under two bias voltages of BC $V_S = 0$ and $V_S = 100V$ at $V_A = 1$ kV. We find that the negative currents I^- decrease extremely in comparison with the case of Fig. 6. As these reasons, we can point out that the apparent increment of I^- due to the positive ions from S.P. is lost (when $V_S > 0$), and that the space charge compensation of the π^- or μ^- particles by the positive ions is lost also along the π^- or μ^- particle orbit inside of MA.

5. Investigation of positive pionlike or muonlike particle

We tried to detect positive pionlike (π^+) or muonlike (μ^+) particles by reversing the polarity of analyzing magnetic field B_M of MA as shown in Fig. 9 (A) and Fig. 9 (B). A dependence of a positive current I^+ to the beam collector BC on the reversed magnetic field ($-B_M$) of MA are

determined in Fig. 10 under three bias voltages of $V_S = 0V$, $V_S = 100V$ and $V_S = -100V$ at the first electron beam acceleration voltage $V_A = 1$ kV. In Fig. 10, we find that the peaks of the positive current I^+ correspond to a positive pionlike particle and a muonlike particle following to Eq. (2) and is very small in comparison with those of Fig. 6 for the π^- or μ^- particles, and that the apparent current does not increase even under $V_S = 100V$ or $V_S = -100V$. Next, a cut plate CP for the secondary plasma S.P. is arranged under the reversed magnetic field ($-B_M$) corresponding to Fig. 8 (A). A dependence of the positive current I^+ to the BC on ($-B_M$) is the same with that of Fig. 10. That is, the dependence of I^+ on ($-B_M$) is not varied by the cut plate CP or the secondary plasma S.P..

From these experimental results of Fig. 10 and Fig. 8 (A) under ($-B_M$), we can conclude that the apparent current increment does not occur for the π^+ or μ^+ particles, and that the space charge compensation effect (which occurs for the π^- or μ^- particles by the positive ions inside MA as shown in Fig. 6) does not occur also for the π^+ or μ^+ particles.

(Even if the introducing gas to the first electron beam region as shown in Fig. 1 and Fig. 2 is from Ar to He or H_2, the positive current peak positions of Fig. 10 for the analyzing magnetic field ($-B_M$) are not varied. Therefore, it is obvious that the positive current peaks of Fig. 10 do not come from some classical positive ions).

7. Discussion

The large apparent current increment of the π^- or μ^- particles are explained[4] from the negative secondary electrons e_S^- which are generated from the negative high energy electron e_H^- due to the μ^- particle decay inside the beam collector (metal) BC. That is, the following processes are considered:

$$\pi^- \rightarrow \mu^- + \upsilon_1 \quad \cdots\cdots (3)$$

$$\mu^- \rightarrow e_H + \upsilon_2 \quad \cdots\cdots (4)$$

$$e_H^- \rightarrow Ne_S^- \text{ in Metal (BC)}, \quad \cdots\cdots (5)$$

where υ_1 and υ_2 are some neutrinos. By these negative secondary electrons Ne_S^- and the positive ions from the secondary plasma S.P. as shown in Fig. 1 and 2, the large apparent current increment will be arised for the beam collector BC under $V_S > 0$.

On the other hand, an apparent current increment of the π^+ or μ^+ particles does not occur. As this reason, we consider the following processes:

$$\pi^+ \rightarrow \mu^+ + \upsilon_1' \quad \cdots\cdots (6)$$

$$\mu^+ \rightarrow e_H^+ + \upsilon_2' \quad \cdots\cdots (7)$$

$$e_H^+ \rightarrow e_M^- \rightarrow \gamma \text{ in Metal (BC)}, \quad \cdots\cdots (8)$$

where e_H^+ is high energy positron due to the μ^+ decay inside the beam collector BC, e_M^- is negative electron in the BC (metal) and γ is a γ ray, and where υ_1' and υ_2' are some neutrinos. That is, the negative secondary electrons e_S^- for the apparent current increment are not produced. Moreover, we must point out that the space charges of π^+ or μ^+ are not compensated (by some negative electrons) inside the analyzing magnetic mass analyzer. Because the negative electrons from the secondary plasma S.P. can not enter into the analyzing (strong) magnetic field region under the magnetron cut off. Thus, it is difficult usually to detect the positive pionlike π^+ or muonlike μ^+ particles while a pair creation of π^+ and π^- is occurred by a large electric field due to the electron bunch and the positive ion bunch.

8. Large net current generation of μ^-

In future, a large net current of the μ^- particles may become important for some industrial uses, especially for the negative muon catalyzed fusion. We can show that large net currents of the μ^- particles generate in the experimental apparatus as shown in Fig. 1 and Fig. 2. By increasing the first electron beam (F.E.B.) current I_A and acceleration voltage V_A, the large net currents (I^- net) of the μ^- particles are generated as shown in Fig. 11 under the beam collector bias voltage V_S = 0V. We expect larger net currents through improvement of the electron gun and adjustment of the neutral gas pressure in the first electron beam region.

9. Additional Confirmation

When the positive ions from S.P. as shown in Fig. 12 diffuse also to the back of the beam collector BC, the I^- peak currents corresponding to the π^- or μ^- particle much decrease below 1/10 in comparison with those for Fig. 2 and Fig. 6. Thus, the penetration phenomena of π^- or μ^- particles for BC are obvious as reported[3] already.

10. Difference of metal plate penetration between π^- (μ^-) and π^+ (μ^+)

A metal plate MP (1 mm in thickness) is arranged in front of the beam collector BC as shown in Fig. 13 (A) and 13 (B). Thus, dependences of the negative current I^- or the positive current I^+ to the beam collector BC on the analyzing magnetic field B_M or the reversed magnetic field ($-B_M$), are determined as shown in Fig. 14. Then, we find that the negative currents I^- of the π^- or μ^- particles appear on the BC and that the positive currents I^+ of the π^+ or μ^+ particles do not appear. That is, the π^+ or μ^+ particles can not penetrate the metal plate MP while the π^- or μ^- particles penetrate the MP as reported already[6].

References

1) J. Uramoto: National Institute of Fusion Science, Nagoya, Japan-Research Report, NIFS-377 (1995).

2) J. Uramoto: NIFS-400 (1996).

3) J. Uramoto: NIFS-414 (1996).

4) J. Uramoto: NIFS- To be reported.

5) J. Uramoto: NIFS-277 (1994).

6) J. Uramoto: NIFS-350 (1995).

Figure Captions

Fig. 1 and Fig. 2: Schematic diagrams of the experimental apparatus.

F: Filament as electron emitter. K: Cathode of electron gun. A: Anode of electron gun. V_A: Initial electron acceleration voltage. I_A: Total negative current. F.E.B.: First electron beam. G: Neutral gas. D: Decelerator of F.E.B. S: Entrance slit (3 mm × 10 mm). Ins: Insulator. I.B.: Ion beam. S.E.B.: Second electron beam. e: Electrons with cyclotron motions. μ^-: Negative muonlike particle. (MA): Mass analyzer. Fe: Iron. C: Magnetic Coil. (N): North pole of electro-magnet. (S): South pole. B_M: Analyzing magnetic field. BC: Beam collector. I^-: Negative current to BC. V_S: Bias voltage of BC with respect to mass analyzer body. S.P.: Secondary plasma inside (MA). X: Entrance of uniform magnetic field. i: Ion bunch. π^-: Negative pionlike particle. Ins: Insulator. +Ion: Positive ion.

Fig. 3 Fringe magnetic field distribution (at 1A of magnetic coil current).

B_M: Analyzing magnetic field of (MA). B_O: Uniform magnetic field inside (MA). X: End of uniform magnetic field. S: Entrance slit position. Fe: Magnetic field distribution in a case using iron plate as D in Fig. 1. Cu: Magnetic field distribution in a case using copper plate as D in Fig. 1.

Fig. 4 Applied electrical potential distribution

V: Electrical potential. V_A: Initial potential (voltage) of electron gun anode. V_E: Effective potential for μ^- (negative muonlike particle) and π^- (negative pionlike particle). e_0: Initial electrons from electron gun cathode. e_1: First electron beam. e_2: Second electron beam. i_1: Positive ion beam from plasma. i_2: Second positive ion beam. e–B: Electron bunch due to magnetic cyclotron motion. i–B: Positive ion bunch due to electrical retardation. K: Cathode position of electron gun. A: Anode position of electron gun. S: Slit position of mass analyzer. X: Entrance position of analyzing uniform magnetic field. $+V_A$: Additional potential generated by stopping the positive ion beam.

Fig. 5 Dependence of the negative beam collector current I^- on the analyzing magnetic field B_M under the initial electron acceleration voltage $V_A = 1$ kV and the total anode current $I_A = 3$ mA.

Beam collector bias voltage $V_S = 100$V. Neutral gas pressure is 1×10^{-4} Torr (Ar gas) in the first electron beam region. μ^-: (means negative muonlike particle). π^-: (means negative pionlike particle). e: (means electron).

Fig. 6 Dependences of I^- on B_M under $V_A = 1$ kV and $I_A = 3$ mA.

(1): $V_S = 0$V. (2): $V_S = 100$V.

Fig. 7 (A) Closed circuit of negative charged particle current under $V_S = 0$V.

I_1^-: Net current of negative charged particle (μ^-, π^-). BC: Beam collector. MA: Magnetic mass analyzer.

(See captions of Fig. 1 and Fig. 2 also).

Fig. 7 (B) Increment circuit of negative current under $V_S > 0$.

+Ion: Positive ions within MA. e_S: Secondary electrons inside BC. I_2^-: Increased negative current.

Fig. 8 (A) Additional schematic diagram of the experimental apparatus.

CP: Cut plate of the secondary plasma S.P..

(See captions of Fig. 1 and Fig. 2 also).

Fig. 8 (B) Dependences of I^- on B_M in a case arranged CP under $V_A = 1$ kV and $I_A = 3$ mA.

(1): $V_S = 0$V. (2) $V_S = 100$V.

Fig. 9 (A) Schematic diagram (1) of the experimental apparatus for detection of positive pionlike (π^+) or muonlike (μ^+) particle.

$-B_M$: Analyzing magnetic field reversed the polarity. I^+: Positive current to the beam collector BC.

(See captions of Fig. 1 and Fig. 2 also).

Fig. 9 (B) Schematic diagram (2) for detection of π^+ or μ^+.

(See captions of Fig. 1, Fig. 2 and Fig. 9 (A) also).

Fig. 10 Dependence of the positive current I^+ to the beam collector BC on the reversed magnetic field ($-B_M$).

Initial electron acceleration voltage V_A = 1 kV. Total anode current I_A = 3 mA. Neutral gas pressure is 1×10^{-4} Torr (Ar) in the first electron beam region. π^+: (means positive pionlike particle). μ^+: (means positive muon particle).

Fig. 11 Dependences of net current I_N^- of μ^- on B_M under various first electron beam acceleration voltages V_A at the first electron beam current I_A = 30 mA.

(1): V_A = 0.5 kV. (2): V_A = 1 kV. (3) V_A = 1.5 kV. μ^-: Negative muonlike particle.

Fig. 12 Schematic diagram of the case where the positive ions diffuse to the back of beam collector BC.

(See captions of Fig. 1 and Fig. 2 also).

Fig. 13 (A) Schematic diagram for metal plate penetration of π^- or μ^-.

MP: Metal plate of 1 mm in thickness.

(See captions of Fig. 1 and Fig. 2 also).

Fig. 13 (B) Schematic diagram for metal plate penetration of the positive pionlike π^+ or muonlike μ^+ particle.

MP: Metal plate (1 mm in thickness).

[See captions of Fig. 1 and Fig. 2, and Fig. 9 (A) and Fig. 9 (B)].

Fig. 14 Dependences of I^- on B_M and I^+ on ($-B_M$).

V_A = 1 kV and I_A = 3 mA. (1): V_S = 0V. (2) V_S = 100V.

*I^+ do not appear.

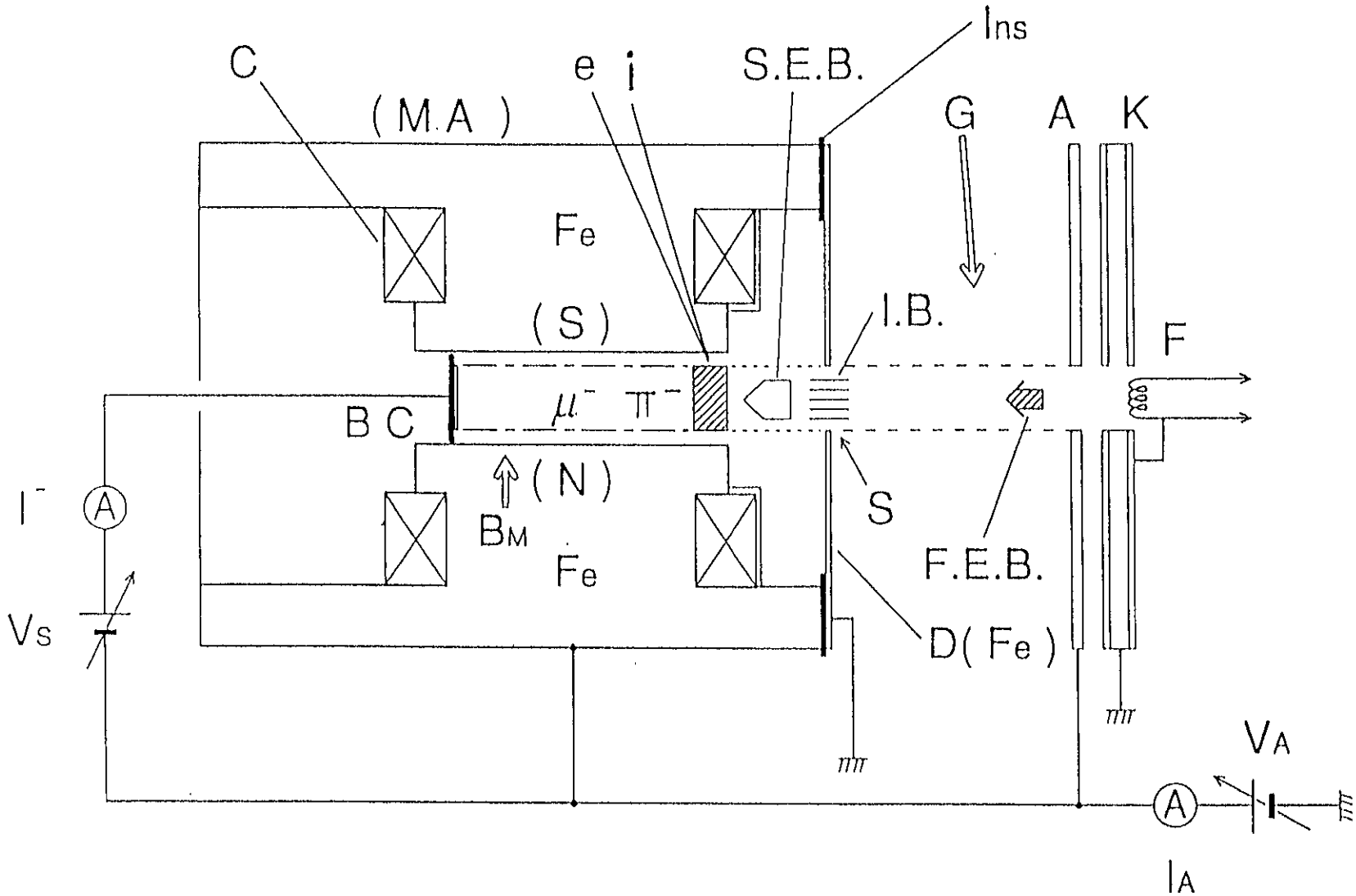

Fig. 1

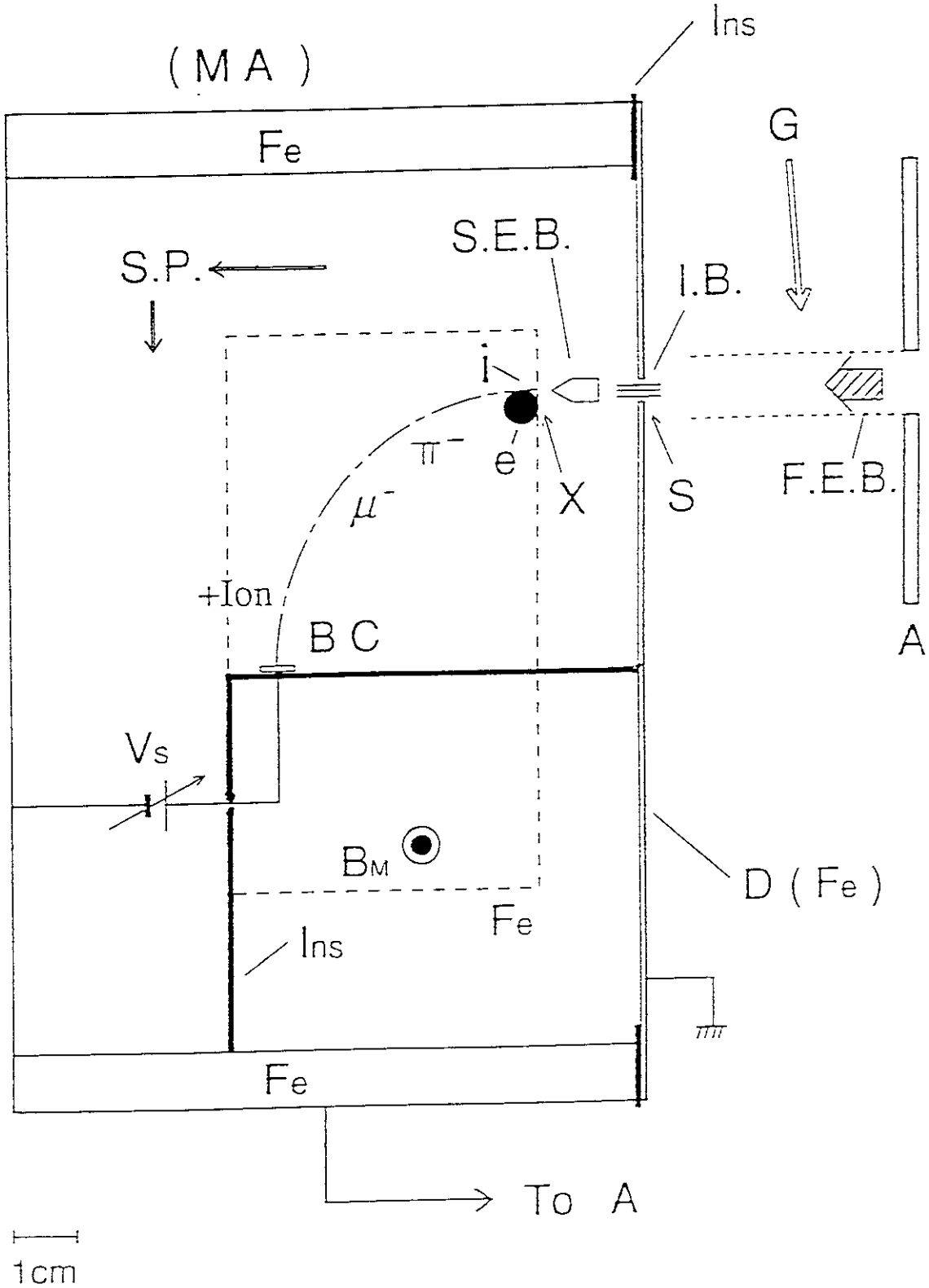
Ins
(M A)
Fe
G
S.E.B.
S.P.
I.B.
i
π⁻
e
μ⁻
X
S
F.E.B.
+Ion
B C
A
Vs
BM
D (Fe)
Fe
Ins
Fe
To A
1cm

Fig. 2

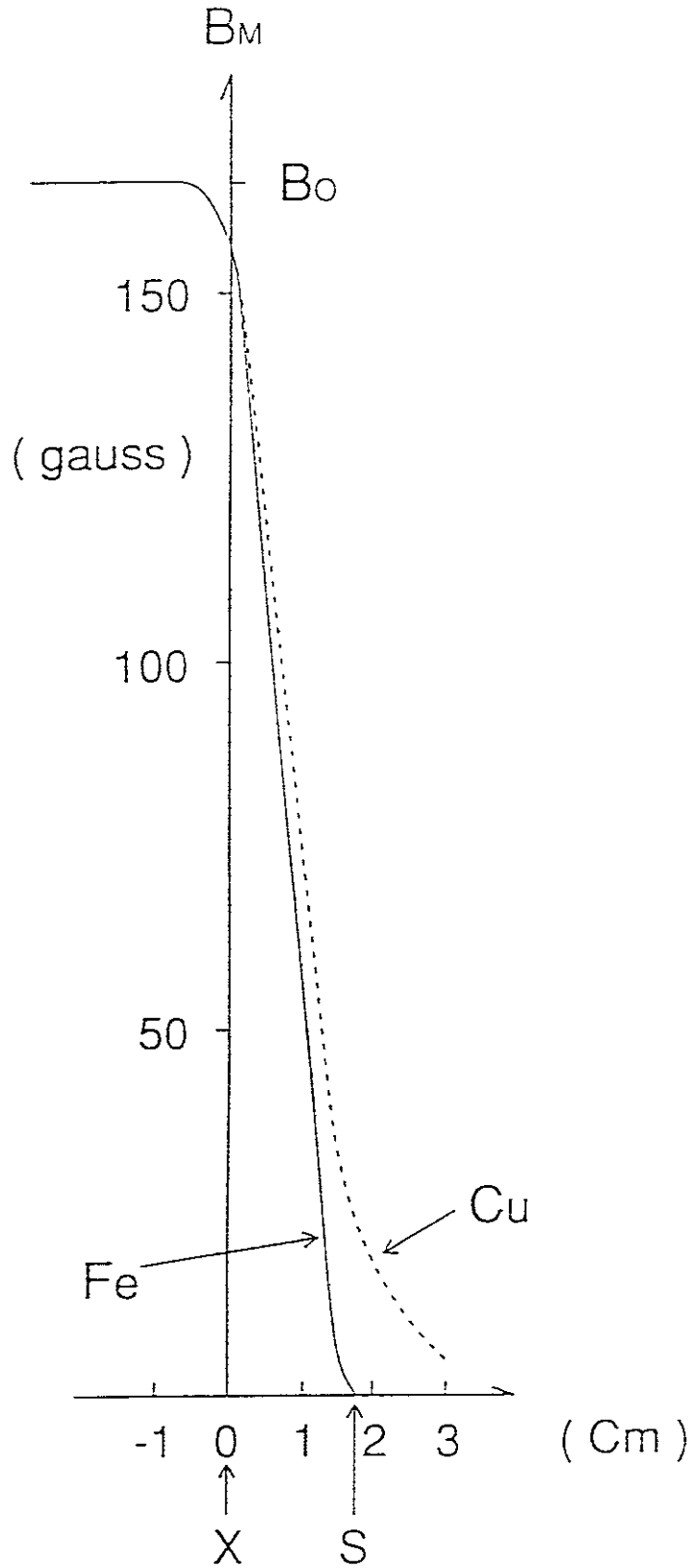

Fig. 3

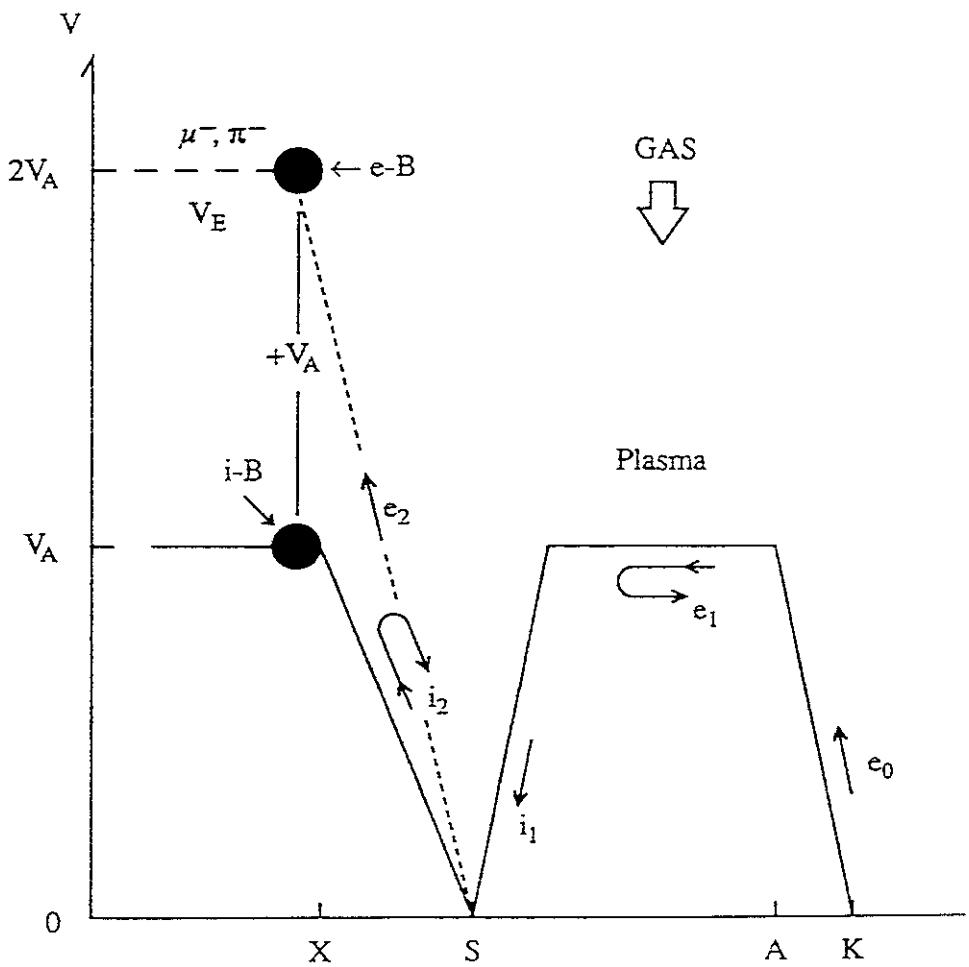

Fig. 4

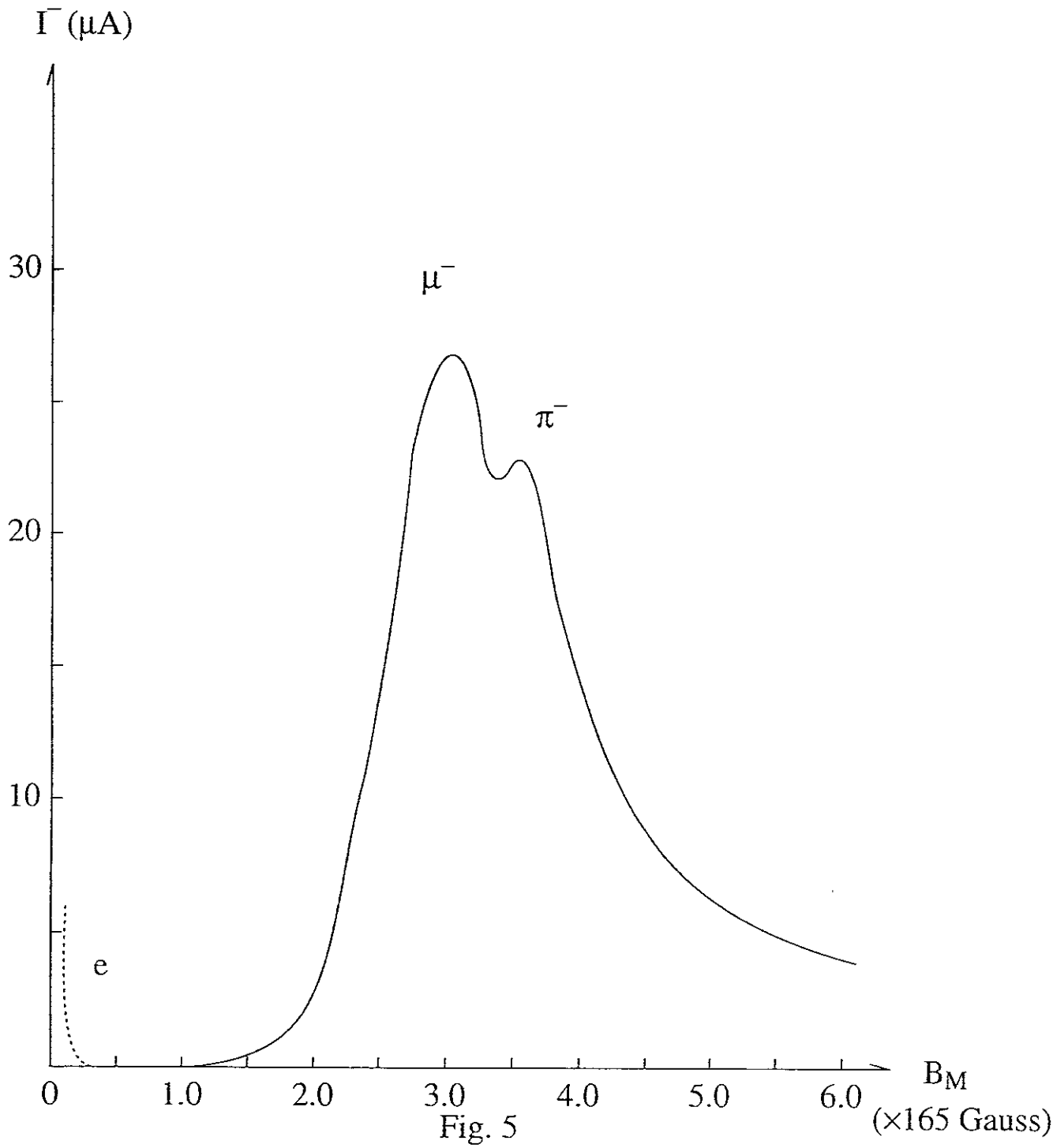

Fig. 5

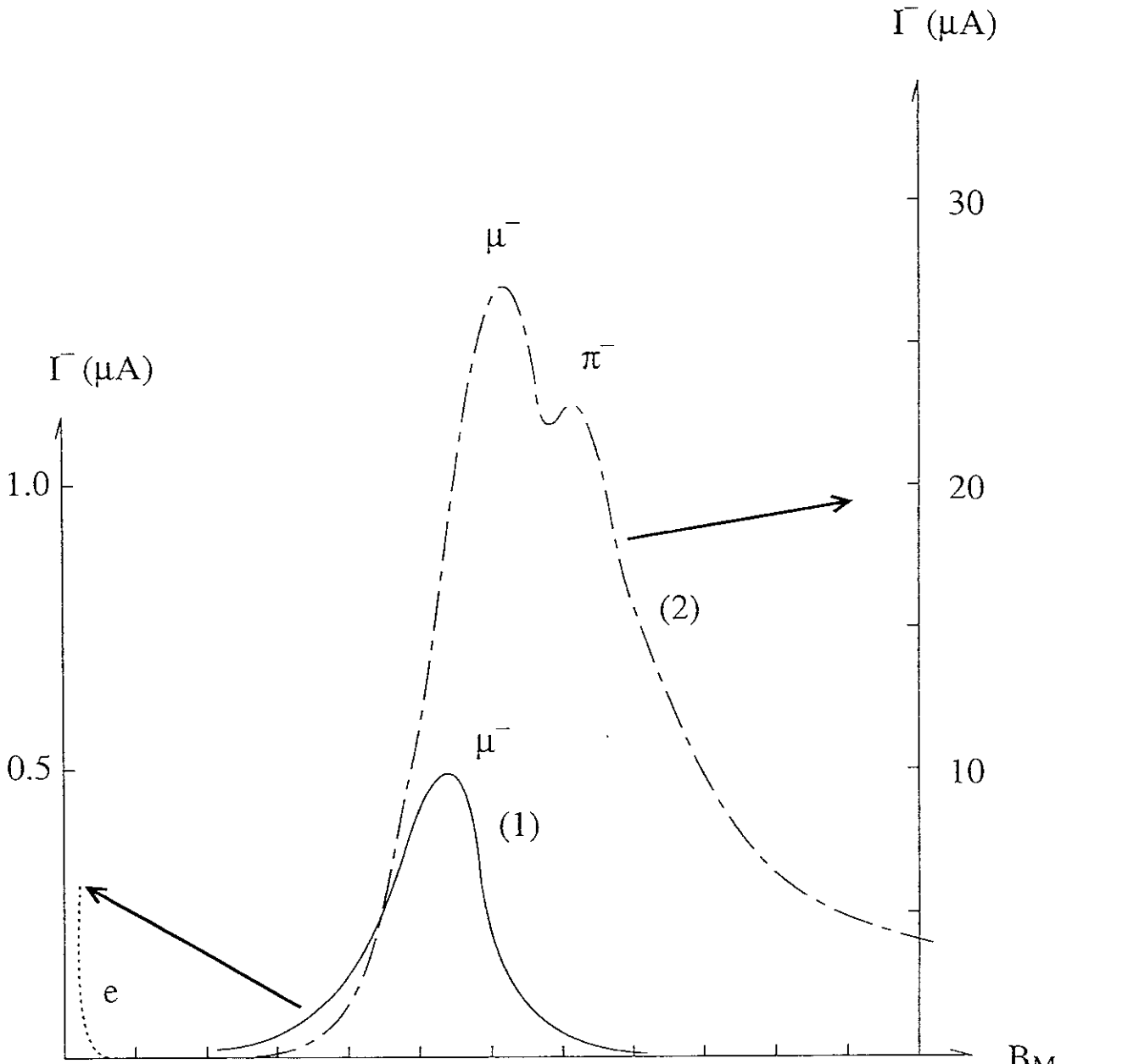

Fig. 6

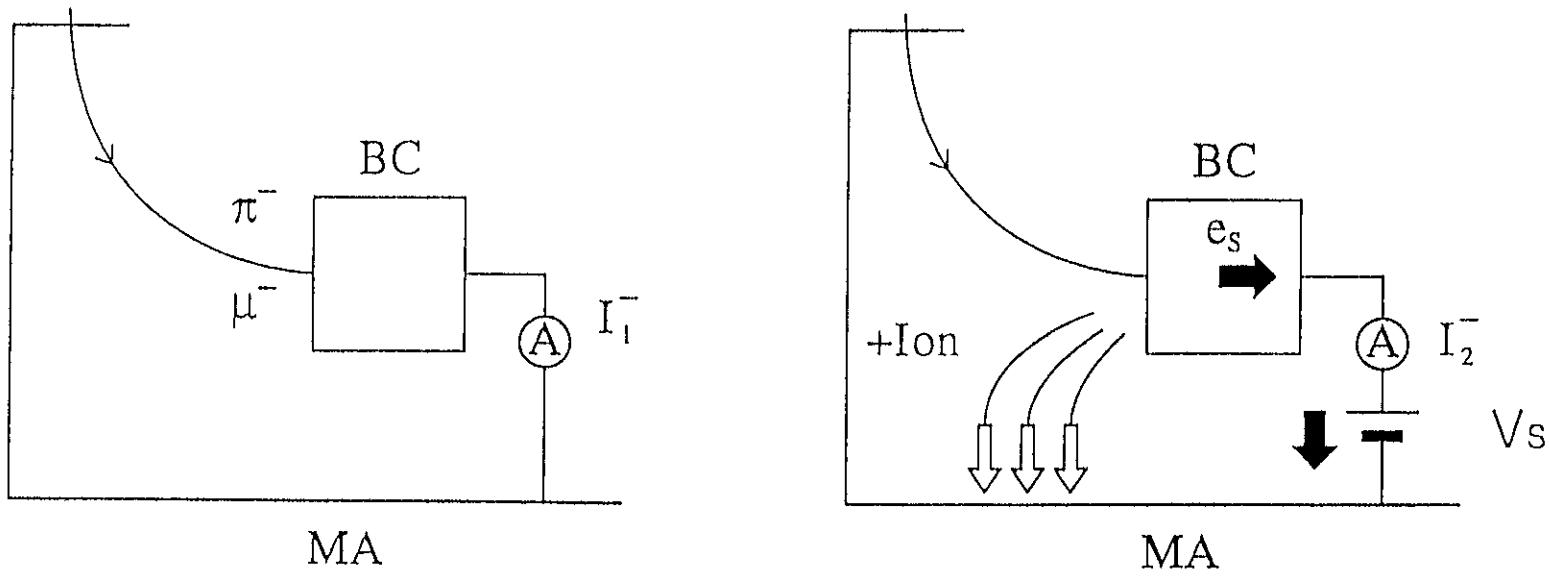

(A) (B)

Fig. 7

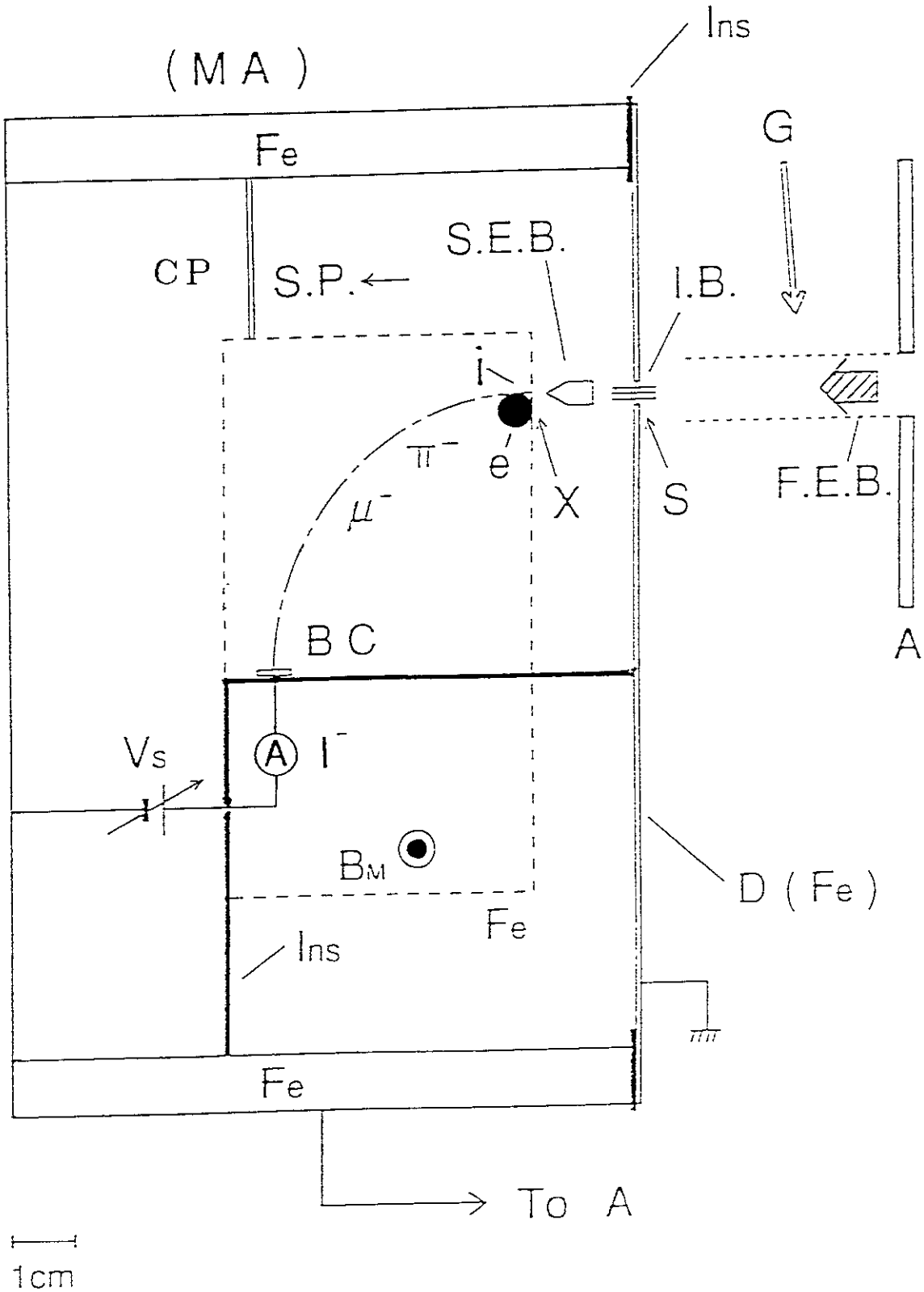
Ins
(MA)
Fe
G
S.E.B.
CP
S.P.←
I.B.
i
π⁻
e
μ⁻
X
S
F.E.B.
A
BC
Vs
A
I⁻
BM
D (Fe)
Fe
Ins
Fe
To A
1cm

Fig. 8 (A)

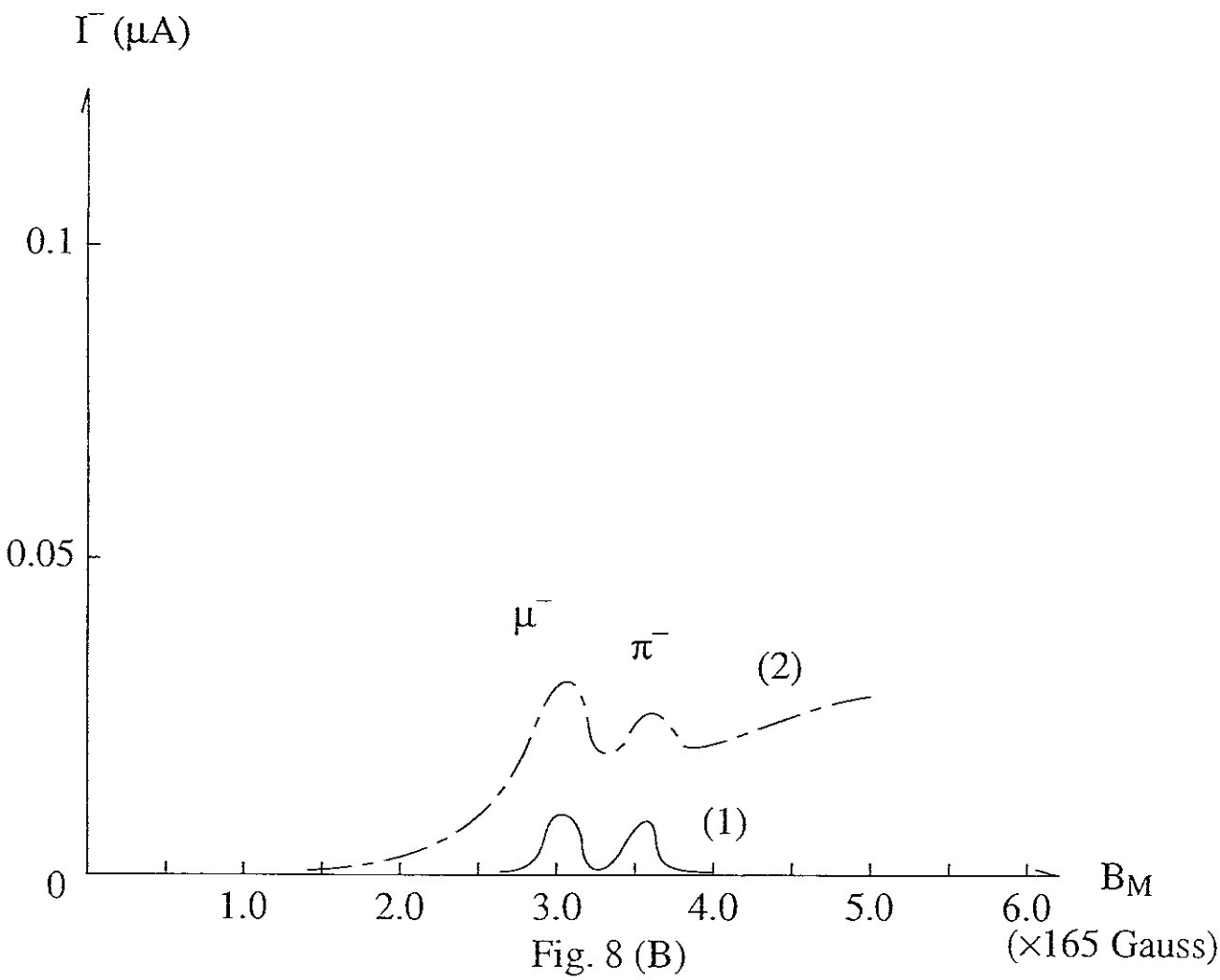

Fig. 8 (B)

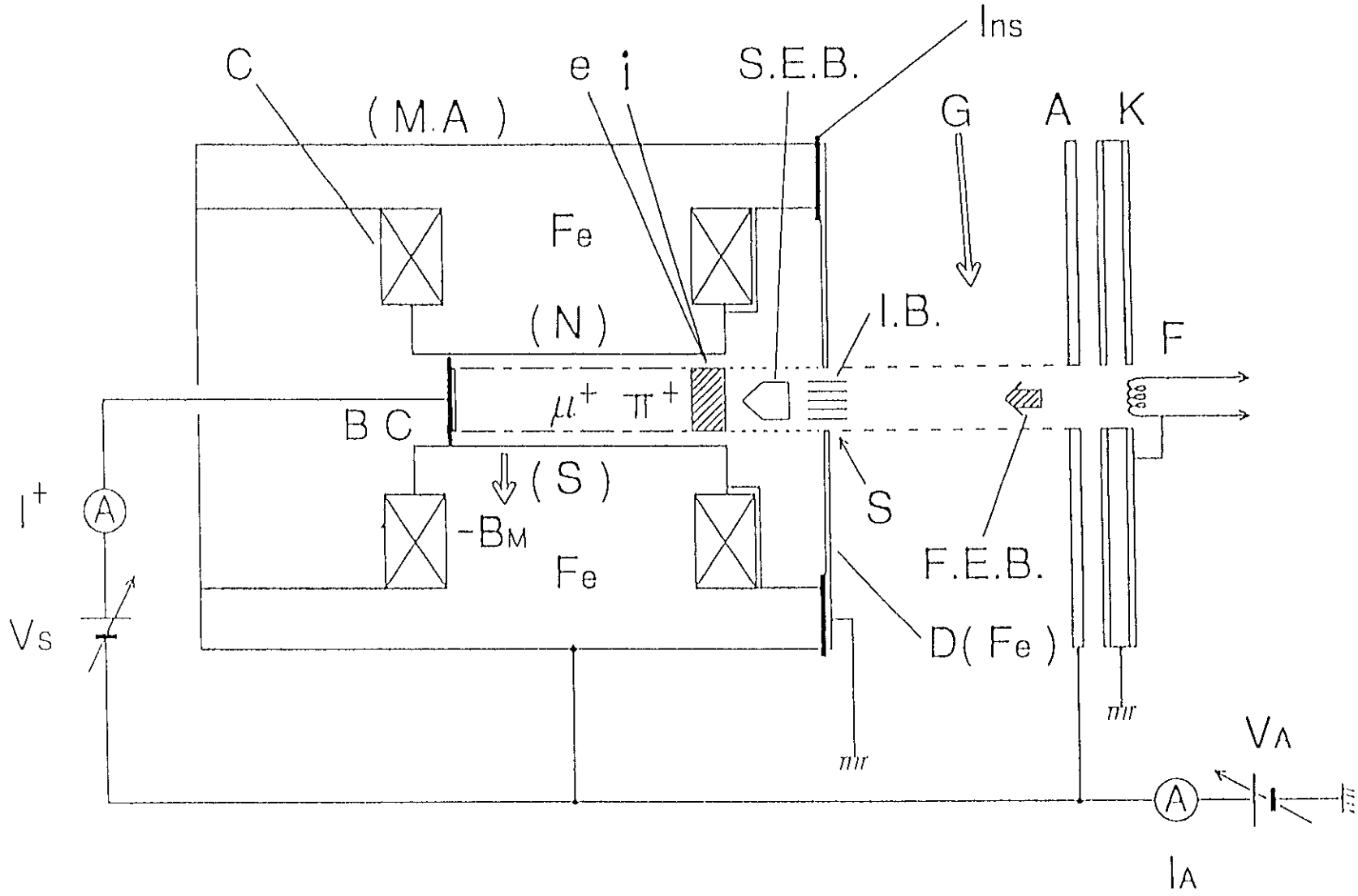
Ins
C
e
i
S.E.B.
(M.A)
G
A
K
Fe
(N)
I.B.
F
μ+
π+
B C
(S)
S
I+
A
-BM
Fe
F.E.B.
Vs
D(Fe)
nir
nir
VA
A
IA

Fig. 9 (A)

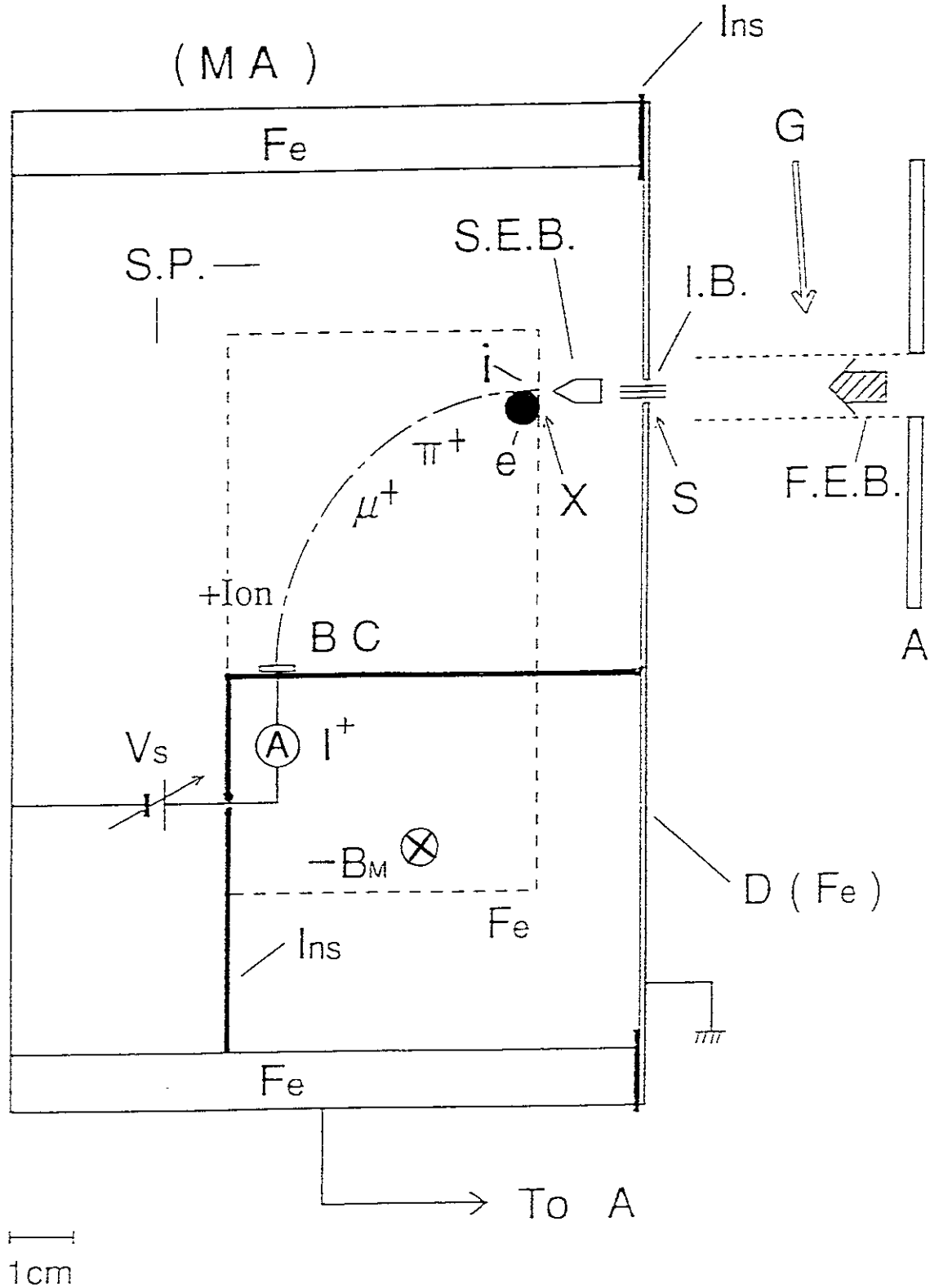
Ins
(MA)
Fe
G
S.E.B.
S.P.
I.B.
i
π+
e
μ+
X
S
F.E.B.
A
+Ion
BC
Vs
A
I+
−BM
D (Fe)
Fe
Ins
Fe
To A
1cm

Fig. 9 (B)

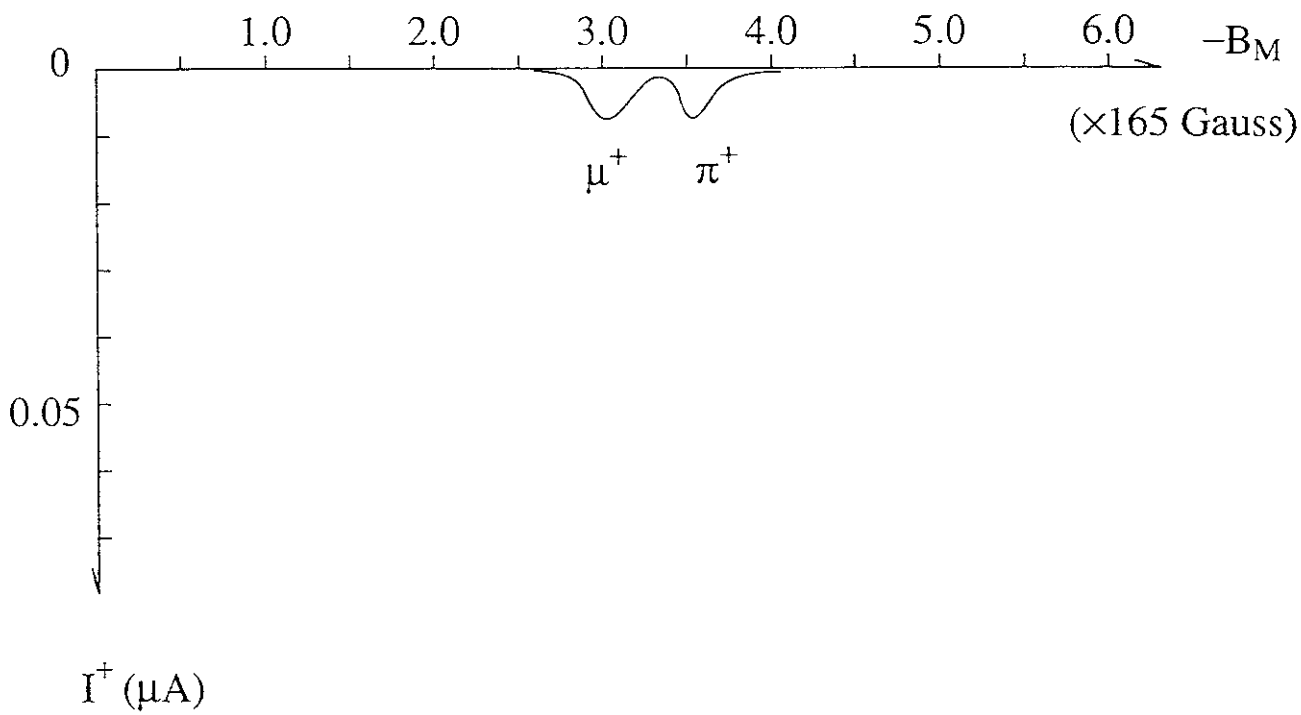

Fig. 10

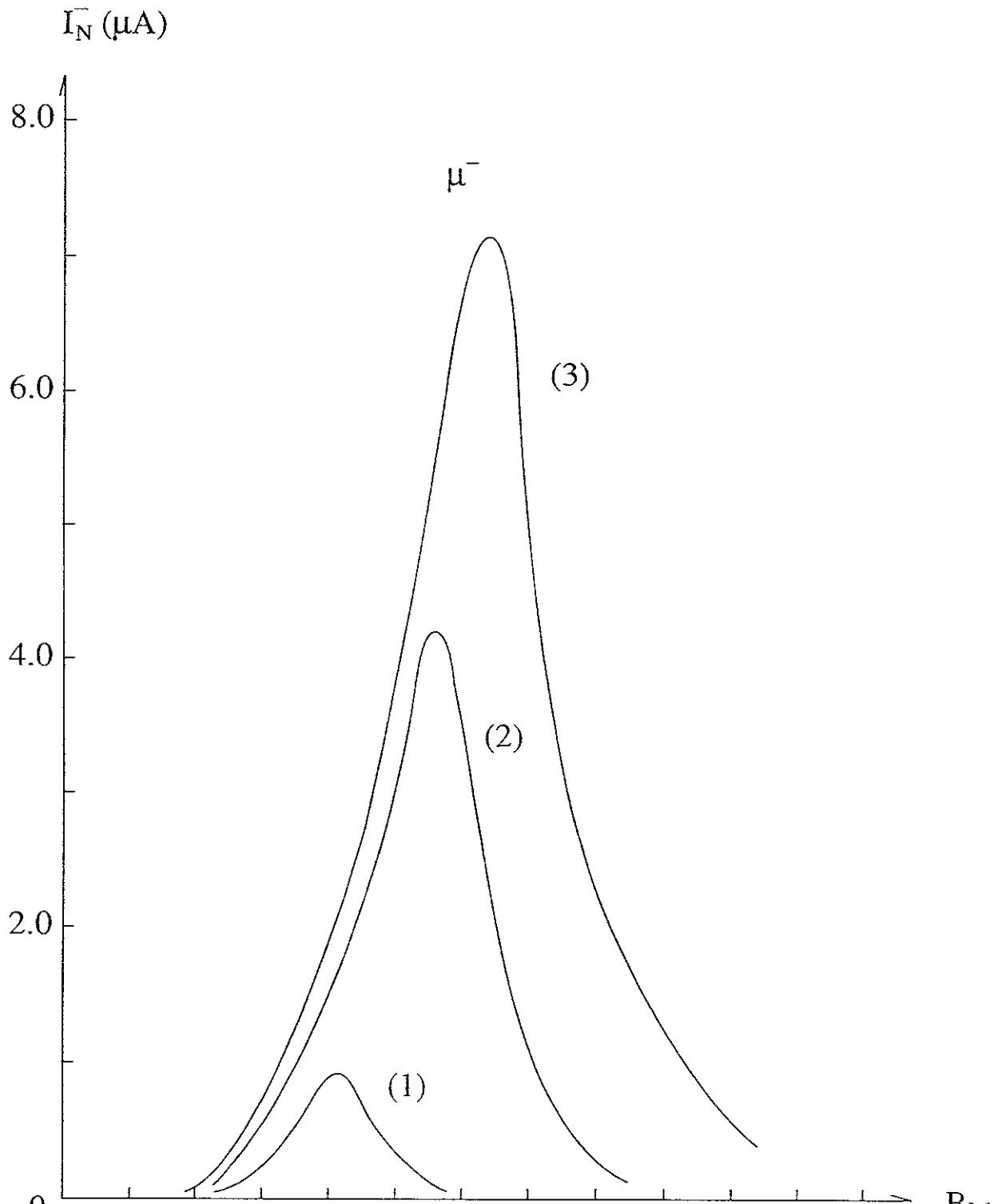

Fig. 11

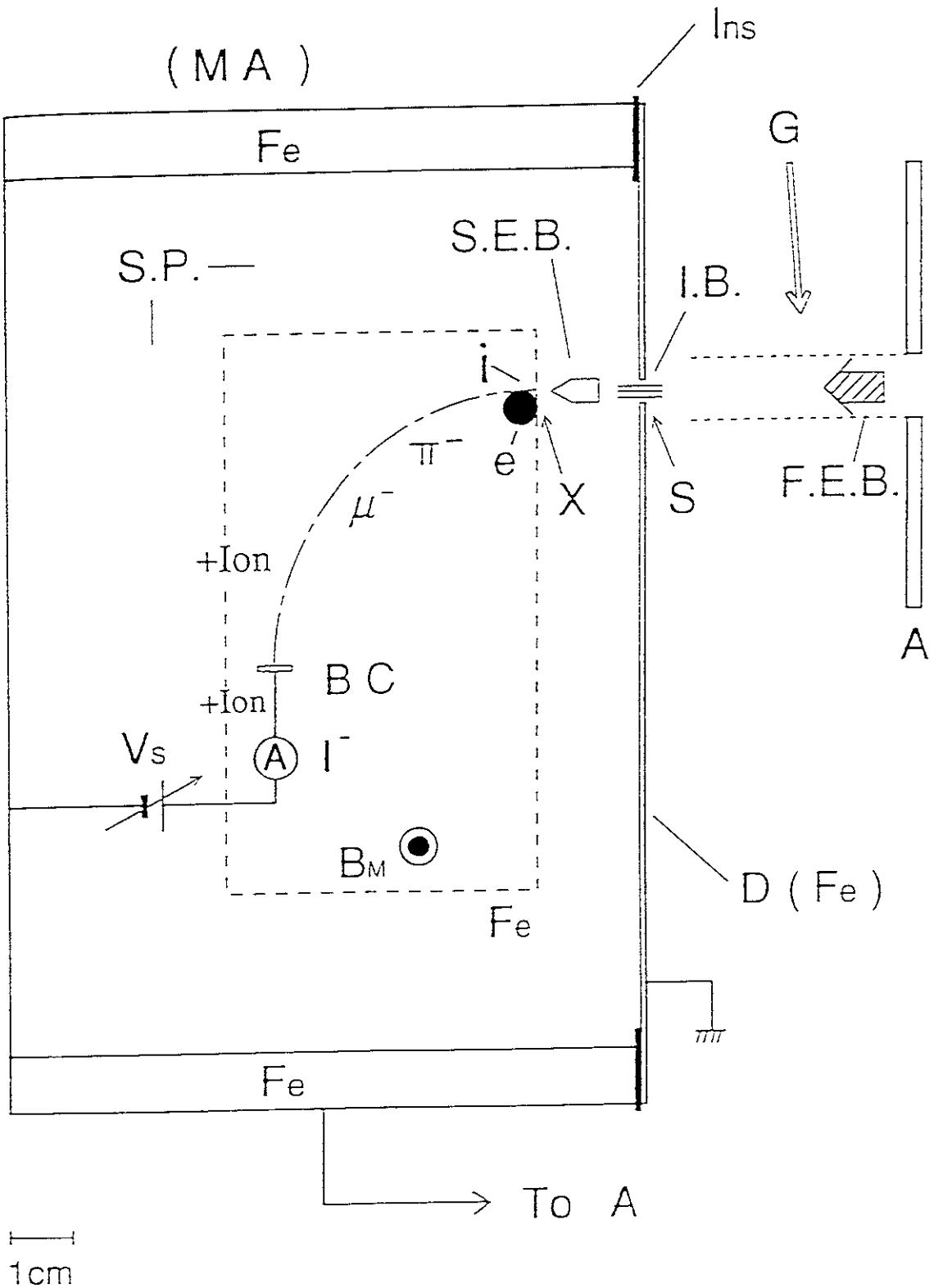
(M A)
Ins
Fe
G
S.P.
S.E.B.
I.B.
i
π⁻
e
μ⁻
X
S
F.E.B.
A
+Ion
B C
+Ion
Vs
A
I⁻
BM
D (Fe)
Fe
Fe
To A
1cm

Fig. 12

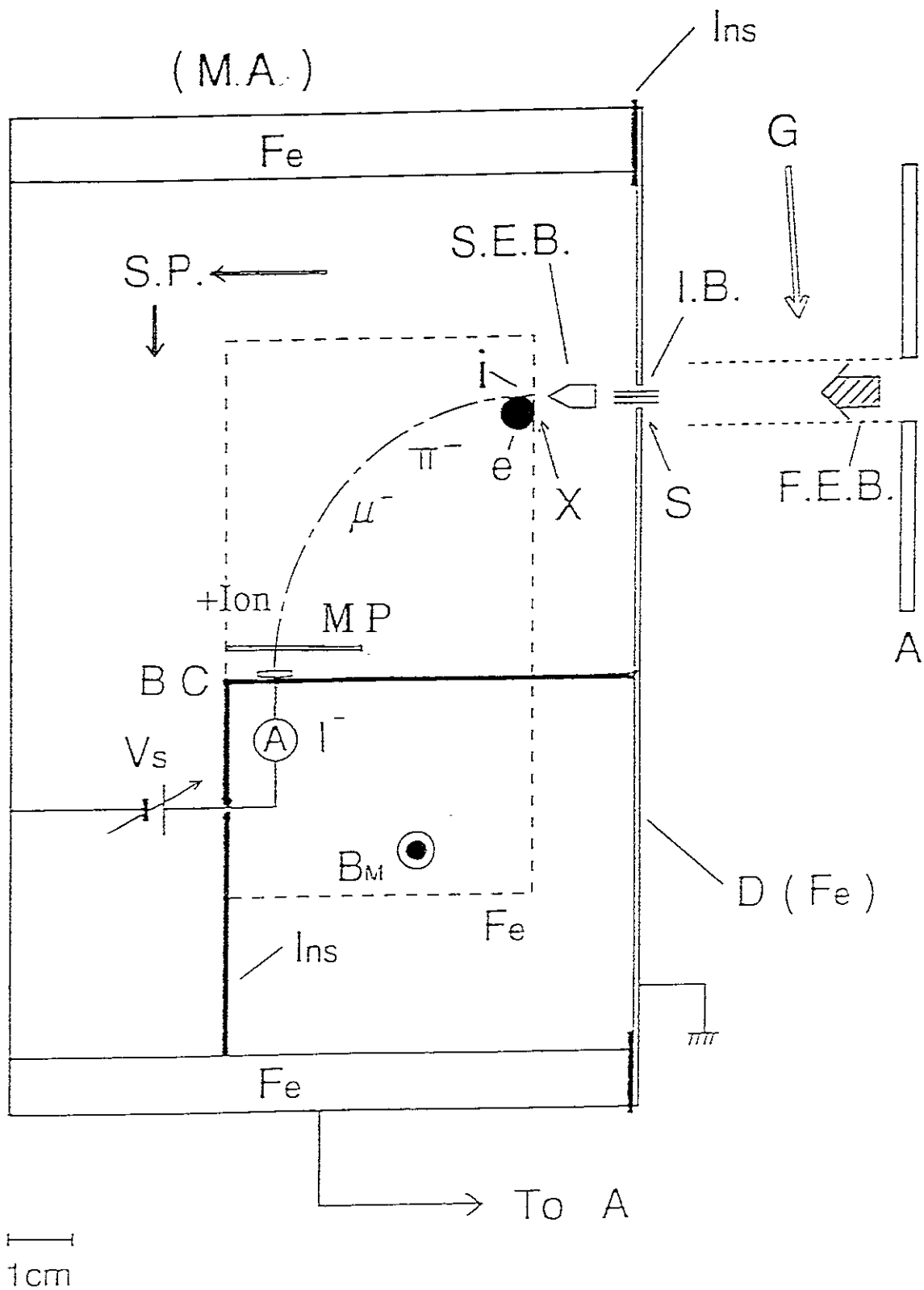
Ins
(M.A.)
Fe
G
S.E.B.
S.P.
I.B.
i
π⁻
e
μ⁻
X
S
F.E.B.
A
+Ion
MP
BC
A
I⁻
Vs
BM
D (Fe)
Fe
Ins
Fe
To A
1cm

Fig. 13 (A)

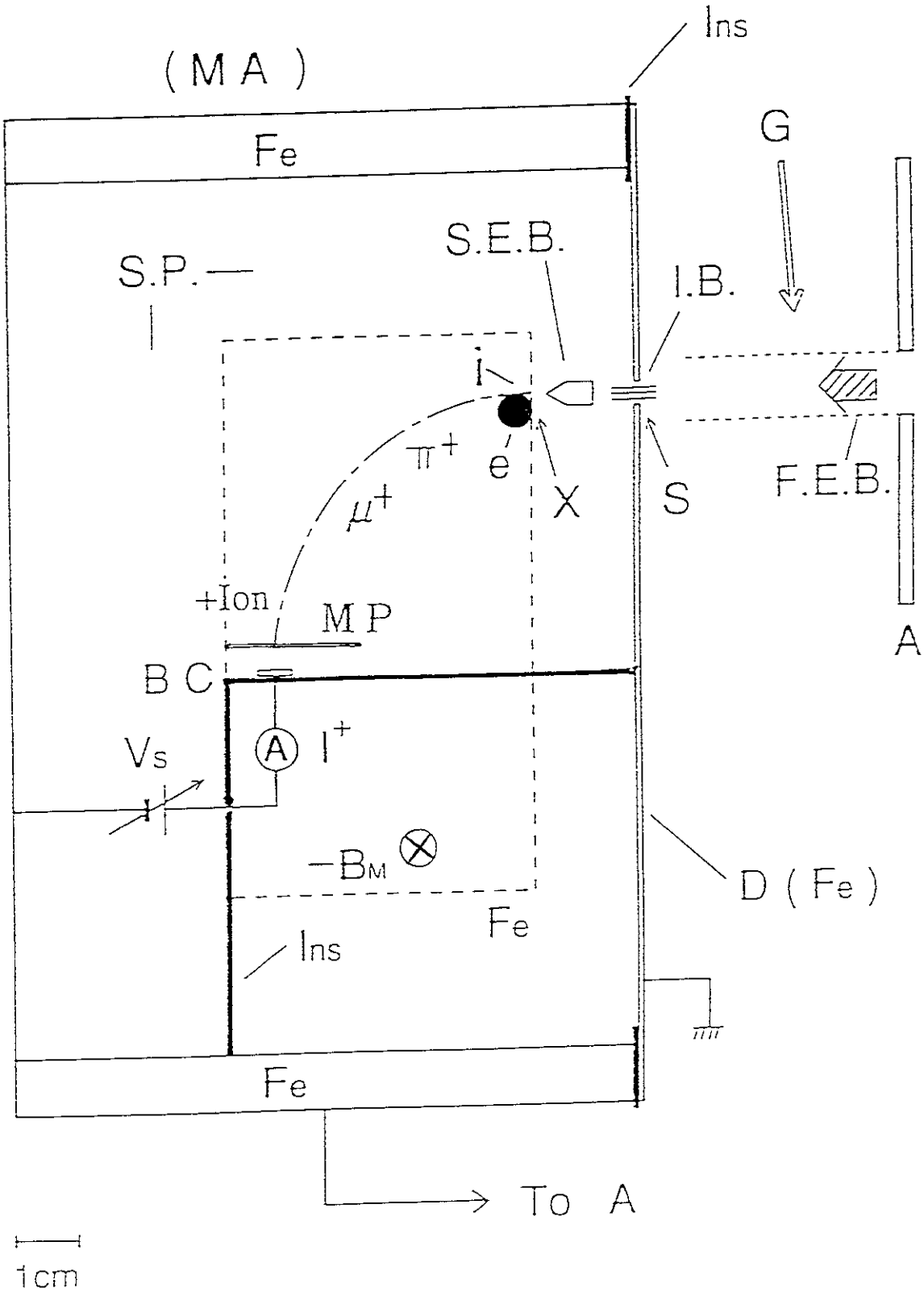
Ins
(MA)
Fe
G
S.E.B.
S.P.
I.B.
i
π+
e
μ+
X
S
F.E.B.
+Ion
MP
A
BC
Vs
A
I+
−BM
D (Fe)
Fe
Ins
Fe
To A
1cm

Fig. 13 (B)

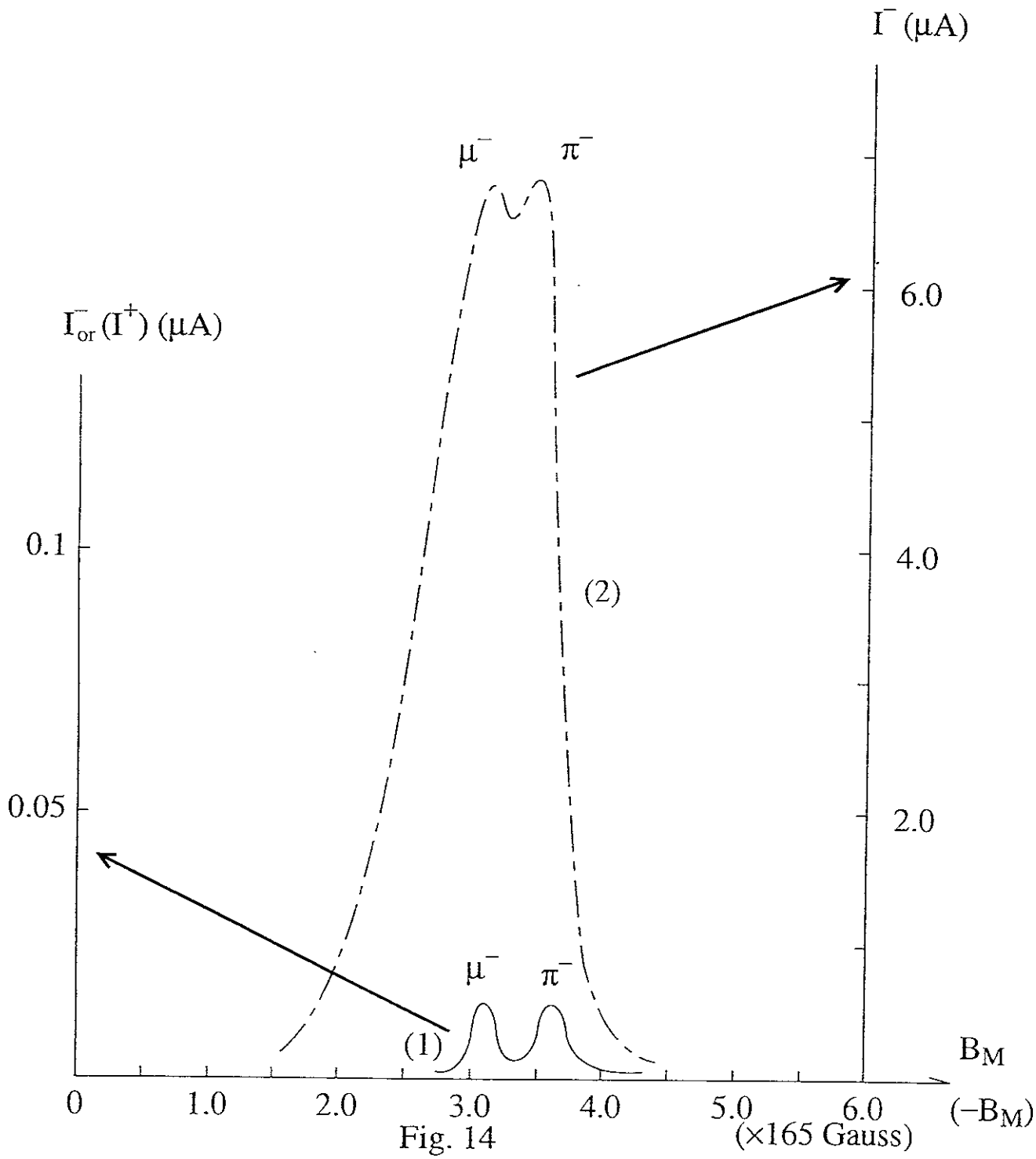
I⁻ (μA)
μ⁻
π⁻
I⁻or (I⁺) (μA)
6.0
0.1
4.0
(2)
0.05
2.0
μ⁻
π⁻
(1)
B_M
0
1.0
2.0
3.0
4.0
5.0
6.0
(−B_M)
(×165 Gauss)

Fig. 14

Recent Issues of NIFS Series

NIFS-489 T Ohkawa
Pfirsch - Schluter Diffusion with Anisotropic and Nonuniform Superthermal Ion Pressure Apr 1997

NIFS-490 S Ishiguro and The Complexity Simulation Group
Formation of Wave-front Pattern Accompanied by Current-driven Electrostatic Ion-cyclotron Instabilities Apr 1997

NIFS-491 A Ejiri K Shinohara and K Kawahata,
An Algorithm to Remove Fringe Jumps and its Application to Microwave Reflectometry, Apr 1997

NIFS-492 K Ichiguchi, N Nakajima M Okamoto,
Bootstrap Current in the Large Helical Device with Unbalanced Helical Coil Currents: Apr 1997

NIFS-493 S. Ishiguro, T Sato, H Takamaru and The Complexity Simulation Group,
V-shaped dc Potential Structure Caused by Current-driven Electrostatic Ion-cyclotron Instability May 1997

NIFS-494 K Nishimura, R Horiuchi, T Sato,
Tilt Stabilization by Energetic Ions Crossing Magnetic Separatrix in Field-Reversed Configuration, June 1997

NIFS-495 T. -H Watanabe and T Sato,
Magnetohydrodynamic Approach to the Feedback Instability, July 1997

NIFS-496 K. Itoh, T Ohkawa S -I Itoh, M Yagi and A Fukuyama
Suppression of Plasma Turbulence by Asymmetric Superthermal Ions July 1997

NIFS-497 T Takahashi, Y Tomita, H Momota and Nikita V Shabrov
Collisionless Pitch Angle Scattering of Plasma Ions at the Edge Region of an FRC, July 1997

NIFS-498 M Tanaka, A Yu Grosberg V S Pande and T Tanaka,
Molecular Dynamics and Structure Organization in Strongly-Coupled Chain of Charged Particles: July 1997

NIFS-499 S Goto and S Kida,
Direct-interaction Approximation and Reynolds-number Reversed Expansion for a Dynamical System, July 1997

NIFS-500 K Tsuzuki N Inoue, A Sagara, N Noda, O Motojima, T Mochizuki, T Hino and T Yamashina,
Dynamic Behavior of Hydrogen Atoms with a Boronized Wall, July 1997

NIFS-501 I Viniar and S Sudo,
Multibarrel Repetitive Injector with a Porous Pellet Formation Unit July 1997

NIFS-502 V. Vdovin, T Watari and A Fukuyama,
An Option of ICRF Ion Heating Scenario in Large Helical Device, July 1997

NIFS-503 E. Segre and S. Kida
Late States of Incompressible 2D Decaying Vorticity Fields, Aug 1997

NIFS-504 S Fujiwara and T Sato,
Molecular Dynamics Simulation of Structural Formation of Short Polymer Chains, Aug 1997

NIFS-505 S Bazdenkov and T Sato
Low-Dimensional Model of Resistive Interchange Convection in Magnetized Plasmas, Sep. 1997

NIFS-506 H Kitauchi and S Kida,
Intensification of Magnetic Field by Concentrate-and-Stretch of Magnetic Flux Lines, Sep 1997

NIFS-507 R L Dewar
Reduced form of MHD Lagrangian for Ballooning Modes, Sep 1997

NIFS-508 Y.-N Nejoh,
Dynamics of the Dust Charging on Electrostatic Waves in a Dusty Plasma with Trapped Electrons, Sep 1997

NIFS-509 E Matsunaga, T Yabe and M Tajima,

Baroclinic Vortex Generation by a Comet Shoemaker-Levy 9 Impact; Sep. 1997

NIFS-510 C.C Hegna and N Nakajima,
On the Stability of Mercier and Ballooning Modes in Stellarator Configurations; Oct. 1997

NIFS-511 K Orito and T. Hatori,
Rotation and Oscillation of Nonlinear Dipole Vortex in the Drift-Unstable Plasma; Oct. 1997

NIFS-512 J. Uramoto,
Clear Detection of Negative Pionlike Particles from H_2 Gas Discharge in Magnetic Field· Oct 1997

NIFS-513 T. Shimozuma, M. Sato, Y. Takita, S. Ito, S. Kubo, H. Idei, K. Ohkubo, T Watari, T.S. Chu, K Felch, P Cahalan and C M Loring, Jr,
The First Preliminary Experiments on an 84 GHz Gyrotron with a Single-Stage Depressed Collector; Oct. 1997

NIFS-514 T Shimozuma, S Morimoto, M Sato, Y Takita, S Ito, S Kubo, H Idei, K Ohkubo and T Watari,
A Forced Gas-Cooled Single-Disk Window Using Silicon Nitride Composite for High Power CW Millimeter Waves; Oct. 1997

NIFS-515 K. Akaishi,
On the Solution of the Outgassing Equation for the Pump-down of an Unbaked Vacuum System; Oct. 1997

NIFS-516 *Papers Presented at the 6th H-mode Workshop (Seeon, Germany)*; Oct. 1997

NIFS-517 John L. Johnson,
The Quest for Fusion Energy, Oct 1997

NIFS-518 J. Chen, N Nakajima and M. Okamoto,
Shift-and-Inverse Lanczos Algorithm for Ideal MHD Stability Analysis, Nov 1997

NIFS-519 M. Yokoyama, N. Nakajima and M. Okamoto,
Nonlinear Incompressible Poloidal Viscosity in L=2 Heliotron and Quasi-Symmetric Stellarators; Nov. 1997

NIFS-520 S Kida and H. Miura,
Identificaiton and Analysis of Vortical Structures, Nov 1997

NIFS-521 K Ida, S. Nishimura, T. Minami, K. Tanaka, S Okamura, M. Osakabe, H Idei, S. Kubo, C. Takahashi and K. Matsuoka,
High Ion Temperature Mode in CHS Heliotron/torsatron Plasmas, Nov. 1997

NIFS-522 M. Yokoyama, N. Nakajima and M. Okamoto,
Realization and Classification of Symmetric Stellarator Configurations through Plasma Boundary Modulations, Dec. 1997

NIFS-523 H. Kitauchi,
Topological Structure of Magnetic Flux Lines Generated by Thermal Convection in a Rotating Spherical Shell; Dec. 1997

NIFS-524 T. Ohkawa,
Tunneling Electron Trap, Dec 1997

NIFS-525 K. Itoh, S -I Itoh, M Yagi, A Fukuyama,
Solitary Radial Electric Field Structure in Tokamak Plasmas· Dec 1997

NIFS-526 Andrey N Lyakhov,
Alfven Instabilities in FRC Plasma, Dec 1997

NIFS-527 J Uramoto,
Net Current Increment of negative Muonlike Particle Produced by the Electron and Positive Ion Bunch-method, Dec. 1997

NIFS-528 Andrey N Lyakhov,
Comments on Electrostastic Drift Instabilities in Field Reversed Configuraiton; Dec. 1997

NIFS-529 J. Uramoto,
Pair Creation of Negative and Positive Pionlike (Muonlike) Particle by Interaction between an Electron Bunch and a Positive Ion Bunch; Dec. 1997